

Congestion in near capacity metro operations: optimum boardings and alightings at bottleneck stations

Anupriya*, Daniel J. Graham, Prateek Bansal, Daniel Hörcher, Richard Anderson

*Transport Strategy Centre, Department of Civil and Environmental Engineering,
Imperial College London, South Kensington, London SW7 2AZ*

Abstract

During peak hours, metro systems often operate at high service frequencies to transport large volumes of passengers. However, the punctuality of such operations can be severely impacted by a vicious circle of passenger congestion and train delays. In particular, high volumes of passenger boardings and alightings may lead to increased dwell times at stations, that may eventually cause queuing of trains in upstream. Such stations act as active bottlenecks in the metro network and congestion may propagate from these bottlenecks to the entire network. Thus, understanding the mechanism that drives passenger congestion at these bottleneck stations is crucial to develop informed control strategies, such as control of inflow of passengers entering these stations. To this end, we conduct the first station-level econometric analysis to estimate a causal relationship between boarding-alighting movements and train flow using data from entry/exit gates and train movement data of the Mass Transit Railway, Hong Kong. We adopt a Bayesian non-parametric spline-based regression approach and apply instrumental variables estimation to control for confounding bias that may occur due to unobserved characteristics of metro operations. Through the results of the empirical study, we identify bottleneck stations and provide estimates of optimum passenger movements per train and service frequencies at the bottleneck stations. These estimates, along with real data on daily demand, could assist metro operators in devising station-level control strategies.

Keywords: urban rail, congestion, causal econometrics, Bayesian machine learning, nonparametric statistics

*Corresponding author. Email address: anupriya15@imperial.ac.uk

1. Introduction

As metro systems around the world face an unprecedented growth in peak-hour ridership, passengers increasingly experience congestion and frequent scheduling delays (Tirachini et al., 2013; Seo et al., 2017). For instance, the London Underground reported 504 congestion-related delays of two minutes or more in 2018 (London Assembly, 2019), and passengers lost almost 400,000 hours due to these delays (Independent, 2017). The congestion in metros can be classified into two main categories: (1) passenger-congestion due to longer boarding and alighting times, and (2) train-congestion due to queuing and reduction in train velocity.

During peak hours, high volumes of passenger boardings and alightings may lead to substantial increases in dwell times of trains at stations, which gives rise to passenger-congestion at stations (Seo et al., 2017). As transit systems are operating at high, often near-capacity service frequencies, increased and irregular dwell times of trains may eventually disrupt service frequencies due to queuing of trains. This queuing phenomenon is referred to as train-congestion or knock-on-delays (Carey and Kwieciński, 1994). Since the headway of train arrivals at stations increase as a result of train-congestion, passenger-congestion at stations intensifies due to further accumulation of passengers on the platform (Seo et al., 2017; Keiji et al., 2015; Daganzo, 2009). Thus, passenger-congestion and train-congestion develop into a vicious cycle, and passenger-congestion is generally the root cause of this phenomenon (Seo et al., 2017; Daganzo, 2009; Zhang and Wada, 2019). The stations where passenger-congestion arises can be characterised as active bottlenecks in the transit network. Based on network configuration and operational attributes, congestion may spread from these bottleneck stations to other parts of the network, resulting in larger overall delays and degradation in system-wide performance.

In recent years, a few studies have modelled the dynamics of metro operations while considering the physical interaction between train-congestion and passenger-congestion (Seo et al., 2017; Zhang and Wada, 2019). A similar literature is available for mainline railway operations (Keiji et al., 2015; Wada et al., 2012, and other references therein). These studies suggest various headway-based control strategies to recover the system from knock-on delays such as keeping a moderate separation between trains with necessary adjustment in departure time from origin stations (Keiji et al., 2015), dwelling time extension at some control stations located at the upstream of the bottleneck station

(Wada et al., 2012) and increase of free flow speed (Daganzo, 2009). However, most of these strategies address train-congestion delays without targeting the root cause of these delays – increased passenger movements at bottleneck stations. Another strand of the literature develops optimisation-based passenger inflow control strategies to minimise the impact of recurrent congestion in metro networks during peak hours. These studies mainly focus on minimising the total waiting time experienced by passengers in the network during peak hours (Shi et al., 2018; Guo et al., 2015; Yuan et al., 2020), reducing the safety risks imposed by passengers waiting on the platform (Jiang et al., 2018; Zou et al., 2018), or minimising the number of stranded passengers (Wang et al., 2020; Yuan et al., 2020).

Unlike previous studies, we focus on understanding the mechanism that drives passenger-congestion at bottleneck stations within an econometric framework. In particular, we aim to estimate a *causal relationship* between the total number of boardings and alightings per train (passenger movements per train, hereafter), and train flows at each station. Since excessive passenger movement at bottleneck stations is the primary driver of congestion, we expect that a *critical passenger movement* level exists in metros at bottleneck stations, above which train flow or throughput of the station reduces. This intuition is analogous to the road traffic flow theory, which presents evidence of a drop in traffic flow through a road section above a critical vehicular density (see Daganzo, 1997, for the fundamental diagram of traffic flow). Therefore, the objective of this exercise is to identify active bottlenecks in the metro network and empirically estimate the optimal passenger movements per train and frequency at bottleneck stations. Such estimates would be instrumental for metro operators in developing data-driven station-based control strategies to avoid both passenger- and train-congestion, and corresponding delays.

To study this congestion phenomenon, we use automated fare collection and train movement data provided by the Mass Transit Railway (MTR), Hong Kong. To find a causal relationship between passenger movements per train and train flows, we adopt an approach that is similar to the estimation of the fundamental diagram of traffic flow in the road traffic theory. However, we argue that estimates derived by simply fitting a pooled ordinary least square regression curve to the observed scatter plot of train flows versus passenger movements per train may be confounded by unobserved characteristics of metro operations such as any existing station-level control measures adopted by the

operator. Moreover, the functional form of the estimated causal relationship is not known a priori. Therefore, we adopt a Bayesian nonparametric instrumental variables (NPIV) approach, proposed by [Wiesenfarth et al. \(2014\)](#), that adjusts for such confounding biases. In addition, we also simulate a synthetic metro system to demonstrate the vicious circle of passenger-train-congestion and the importance of estimating optimal passenger movements in developing station-level control strategies. While the main focus of this study remains station-level empirical analysis, the objective of the simulation study is to provide an intuitive depiction of rail operations using time-space diagrams and illustrate the implications of our empirical analysis in practice.

To summarise, this paper contributes with the first station-level empirical analysis of congestion phenomenon in a metro network. Using the estimated relationship between passenger movements and train flow, we identify potential bottleneck stations. We also provide novel estimates of optimal passenger movements at these stations, which could be instrumental for metro operators to develop informed station-level control strategies.

The rest of this paper is organised as follows. Section 2 presents microsimulation of a synthetic metro system under various control strategies. Section 3 explains the econometric method used in this study and describes the data processing and summary statistics of important variables. Section 4 presents the results of the empirical study. Conclusions and policy relevance of results are discussed in the final section.

2. Simulation of passenger congestion and delays

In this section, we reproduce the passenger-train-congestion phenomenon by simulating a typical high-frequency metro operation under pure moving block signalling system¹. We adopt the model parameters from the study by [Yan et al. \(2012\)](#), which simulates an Asian metro system with near capacity operations. We merge the train operation model from [Yan et al. \(2012\)](#) with a train dwell time model proposed by [Zhang and Wada \(2019\)](#) and [Seo et al. \(2017\)](#) to develop our simulation model. We use this simulation model to demonstrate the efficacy of station-level passenger inflow control measures in avoiding

¹We consider a moving block signalling system over a fixed block signalling system as the former permits a more efficient management of queuing and delays by allowing trains to operate at lower headways ([Gill, 1994](#); [Takeuchi et al., 2003](#)). Several metro lines on the London Underground, the Singapore MRT, the Hong Kong MTR and the New York City subway, among others, use moving block signalling system. Metro systems around the world are increasingly upgrading to such systems to reduce congestion-related delays in the network ([Hong Kong MTR, 2019](#)).

congestion-related delays. The rest of this section is divided into three sub-sections. We describe the train operation model, followed by the main model parameters and the results of the simulation exercise.

2.1. The train operation model

To simulate the movement of trains between stations, we adopt a Cellular Automata (CA) model. The CA model was originally developed for simulation of road traffic flow (Nagel and Schreckenberg, 1992). However, owing to its ability to reproduce complex real world traffic flow phenomena in a simplistic framework (for instance, see Spyropoulou, 2007; Meng and Weng, 2011), it has also been widely used to simulate rail traffic flow (refer to Li et al., 2005; Yinping et al., 2008; Xun et al., 2013; Ning et al., 2014, and other references therein).

In the CA model, the rail line i is divided into L cells, each of length 1 metre (that is, $i \in \{1, 2, \dots, L\}$). The simulation time T_s comprises of discrete time steps t of 1 second each (that is, $t \in \{1, 2, \dots, T_s\}$). At each time step t , each cell i can either be empty or occupied by the n^{th} train with integer velocity $v_{n,t}$ (that is, $v_{n,t} \in \{0, 1, \dots, v_{max}\}$). Stations are placed at different positions along the line and corresponding dwell time is defined. Each train n is indexed based on its order of entry into the system (that is, $n \in \{1, 2, \dots, N\}$). The position of train n at time t is denoted by $X_{n,t}$. The boundary conditions are open and defined as follows: (i) After each departure interval D , a train with velocity v_{max} enters at the position $i = 1$ given that the train ahead is at a safe breaking distance (given by equation 1) from the entry; (ii) At position $i = L$, trains simply exit the system.

At each discrete time step, $t \rightarrow t + 1$, the state of the system is updated according to well-defined rules, mainly governed by the following two situations:

- When the $(n-1)^{\text{th}}$ train is in front of the n^{th} train at time t , a comparison of the headway distance $\Delta X_{n,t} = X_{n-1,t} - X_{n,t}$ and the minimum instantaneous distance $d_{n,t}$ determines whether the n^{th} train will accelerate or decelerate in the next time step. The minimum instantaneous distance between successive trains operating under pure moving-block signalling is given by (Yan et al., 2012):

$$d_{n,t} = \frac{v_{n,t}^2}{2b} + SM \quad (1)$$

where, $v_{n,t}$ is the velocity of train n at time t and b is its deceleration. The first

term on the right hand side of equation 1 represents the breaking distance of train n at time t . A safety margin, SM , is introduced to avoid collision.

- When the n^{th} train is behind an empty station within the breaking distance, its velocity must vary such that the train can stop at the station. To obtain the updated velocity, we apply the kinematics equation: $v_{n,t+1}^2 - v_o^2 = 2bG_{n,t}$, where v_o is the target velocity which is zero for the train to stop at the station and $G_{n,t}$ is the distance between the station and the train n at time t . As the CA model allows only for integer values of velocity, the velocity update $v_{n,t+1}$ is given by:

$$v_{n,t+1} = \text{int}(\sqrt{2bG_{n,t}}) \quad (2)$$

Therefore, the update rules for velocity and position of a train at each time step are as follows:

1. When the n^{th} train is behind the $(n-1)^{\text{th}}$ train

Step 1 Velocity update:

if $\Delta X_{n,t} > d_{n,t}$, $v_{n,t+1} = \min(v_{n,t} + a, v_{\max})$;

elseif $\Delta X_{n,t} < d_{n,t}$, $v_{n,t+1} = \min(v_{n,t} - b, 0)$;

else $v_{n,t+1} = v_{n,t}$.

Step 2 Position update:

$$X_{n,t+1} = X_{n,t} + v_{n,t+1}.$$

2. When the n^{th} train is behind a station

- (a) When the station is occupied by the $(n-1)^{\text{th}}$ train

The update rules are the same as case 1.

- (b) When the station is empty

Step 1 Velocity update:

if $G_{n,t} > d_{n,t}$, $v_{n,t+1} = \min(v_{n,t} + a, v_{\max})$;

elseif $G_{n,t} < d_{n,t}$, $v_{n,t+1} = \min(v_{n,t} - b, \text{int}(\sqrt{2bG_{n,t}}), 0)$;

else $v_{n,t+1} = v_{n,t}$.

Step 2 Position update:

$$X_{n,t+1} = X_{n,t} + v_{n,t+1}.$$

3. When the n^{th} train is at a station

Step 1 Velocity update:

if $t_{dwell} = T_d$ and $\Delta X_{n,t} > L_s$, $v_{n,t+1} = \min(v_n + a, v_{max})$, $t_{dwell} = 0$;
 elseif $t_{dwell} < T_d$, $v_{n,t+1} = 0$, $t_{dwell} = t_{dwell} + 1$.

Step 2 Position update:

$$X_{n,t+1} = X_{n,t} + v_{n,t+1}.$$

where $L_s = \frac{1}{2a} + SM$ is the safe distance to avoid any collision with the train ahead of the dwelling train, t_{dwell} stores the current dwell time (that is, the time for which the train has stopped at the station until time-step t), and T_d is the planned dwell time.

2.2. Model parameters

We consider a metro line of length $L = 4000$ metres with three stations, namely Station 1, Station 2 and Station 3. These stations are located at positions 1000 metres, 2000 metres and 3000 metres respectively. The system is simulated for $T_s = 3600$ seconds. Based on the characteristics of the Asian metro system, we assume that the velocity $v_{n,t}$ of a train in our system varies between 0 and 20 m/s, its acceleration is $a = 1$ m/s², and its deceleration is $b = 1$ m/s² (Yan et al., 2012). We consider that the safety margin is $SM = 50$ metres. We assume that the dwell time of trains at Station 1 T_{d_1} and Station 2 T_{d_2} is 30 seconds. We consider Station 3 as an active bottleneck station along the simulated metro line where the dwell time T_{d_3} increases with increasing passenger movements per train N_p (that is, the total boarding and alighting movements). Consistent with Zhang and Wada (2019) and Seo et al. (2017)), we assume that $N_p = A_p H$, where A_p represents the passenger movement rate and H is the time headway of successive trains at Station 3. Following Zhang and Wada (2019) and Keiji et al. (2015), we adopt the following dwell time model for Station 3:

$$T_{d_3} = \begin{cases} 40 \text{ seconds,} & \text{if } (A_p H \leq N_o) \\ 40 + \gamma(A_p H - N_o) \text{ seconds,} & \text{if } (A_p H > N_o) \end{cases}$$

that is, T_{d_3} remains constant until a critical passenger number N_o is reached, following which it starts increasing. γ represents the growth rate of dwell time with the increase in number of passenger movements. We consider γ to be equal to 0.1. Moreover, we assume that the passenger movement rate A_p increases gradually from a value of 0 passenger per second to a maximum value of 10 passengers per second, with an increment of 0.005

passenger per second at each time step.

Furthermore, we assume that the interval D of trains entering into metro system decreases by 5 seconds at every 2 minutes interval, starting from a value of 120 seconds until it attains a value of 60 seconds. This specification implies that with increasing passenger movements, the operator increases train departure frequency up to the maximum value or the capacity value beyond which further increase in frequency is not possible.

2.3. Results of simulation

Figure 1a shows a time-space diagram representing the train trajectories during the simulation period. From this figure, we note that longer station dwell time of trains at Station 3 eventually leads to queuing of trains or train-congestion in upstream of Station 3, starting at about $t = 2100$ seconds. The queuing-related delays increase the time headway of arrivals of trains at Station 3, which leads to increase in passenger movements because $N_p = A_p H$. As a consequence, station dwell time at Station 3 increases further and queuing of trains in the upstream increases significantly. Based on the spacing of trajectories downstream of Station 3, we note that the throughput of the line first increases as a result of increase in train departure frequency. However, with increasing passenger congestion and delays, this throughput decreases substantially. The number of trains that pass through the system is 39 in an hour.

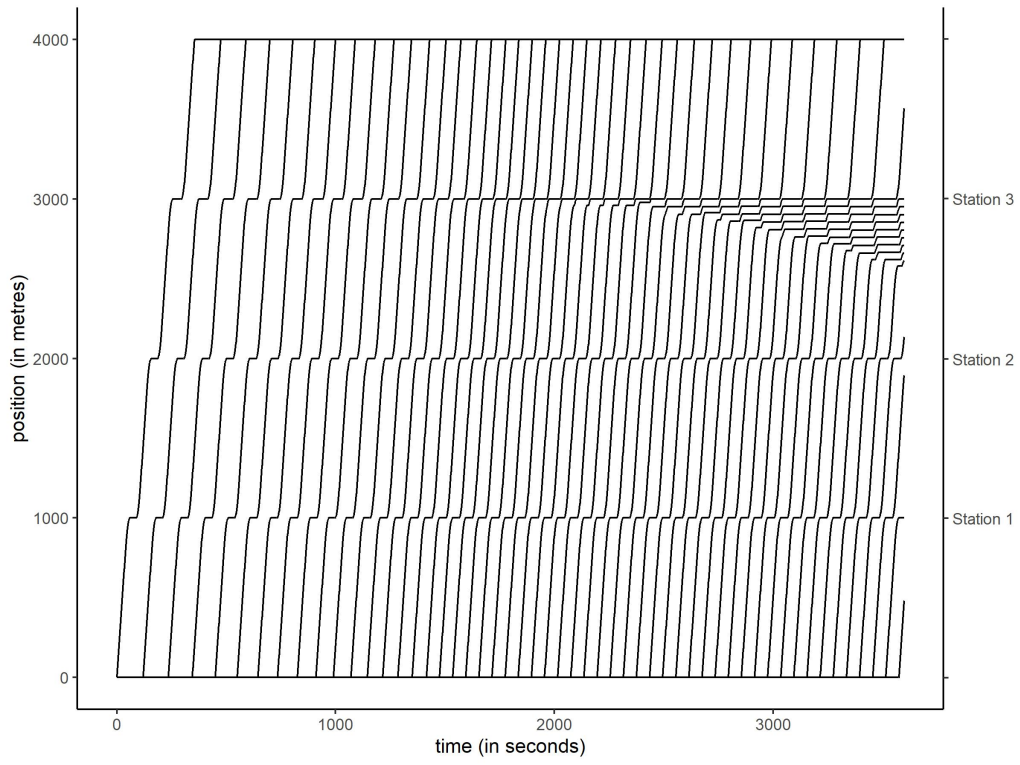
Figure 1b shows the effect of increasing passenger movements per train on train flow at Station 3, where train flow is obtained by taking the inverse of time headway of trains arriving at Station 3. The figure illustrates that with increasing passenger movements, train flow first increases as a result of increase in train departure frequency. However, beyond a certain value of passenger movements, train flow decreases due to high levels of passenger-train-congestion. The maximum observed train flow is 0.0167 train per second and the corresponding optimum level of passenger movements per train is around 580 passengers per hour. Using $N_p = A_p H$, the optimum passenger movement rate turns out to be 9.65 passengers per second.

We now consider two passenger inflow control scenarios: (i) when the passenger movement rate is restricted at 9.75 passengers per second (that is, slightly higher than the optimum rate), and (ii) when the passenger movement rate is restricted at the estimated optimal value of 9.65 passengers per second using station-level control strategies. Figure 2 shows the time-space diagram for both scenarios. Although we observe lower train-

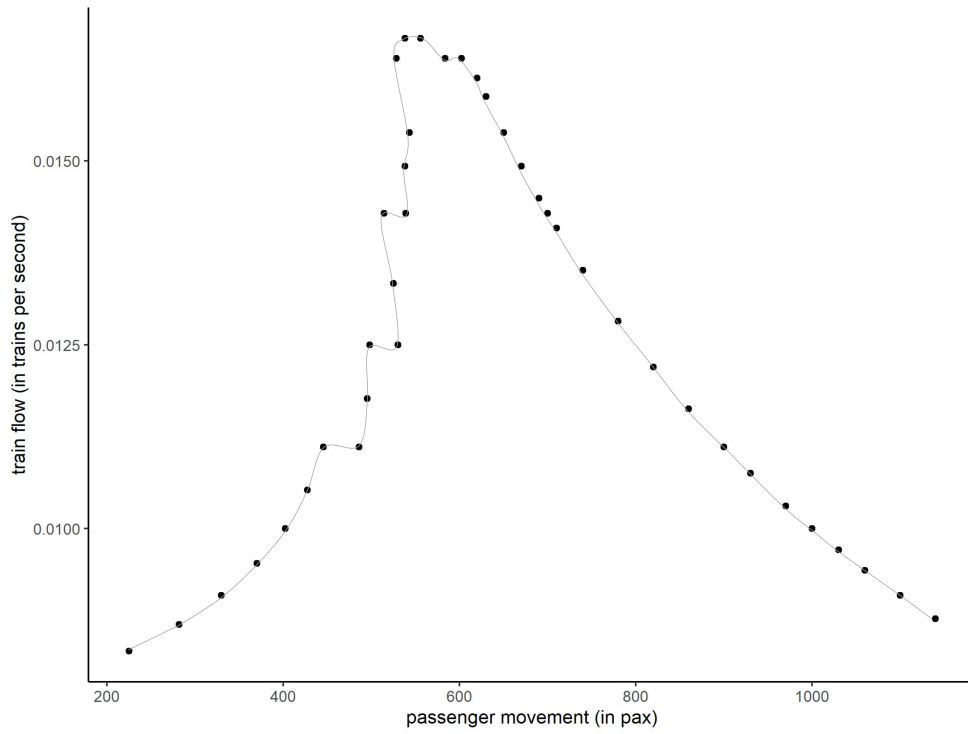
congestion as compared to the *no control* scenario (compare Figures 1a and 2a), train queuing and decrease in system throughput as compared to optimal are still substantial. The number of trains that pass through the system in the first scenario is 43 per hour. Interestingly, the queues are entirely eliminated, and the hourly system throughput increases to 47 trains in the optimal scenario (see Figure 2b).

Furthermore, we compare the station-level passenger inflow control and headway-based control strategies. The headway-based strategies have been recommended in the literature (for instance, see Seo et al., 2017; Keiji et al., 2015), which enable operators to avoid train-congestion by moderating train movements per train. In our headway-based strategy, we control train movements by increasing the interval D between successive trains entering into the metro system. In this controlled scenario, we set the minimum value of D as 90 seconds, as opposed to 60 seconds in the *no control* scenario. Moreover, to avoid queuing, we allow trains to be held longer at stations upstream of the bottleneck (that is, at stations 1 and 2) by increasing their dwell time from 30 seconds to 60 seconds. Figure 3 shows the time-space diagram for this headway-based control scenario. We note that train-congestion is significantly lower in the headway-based control as compared to the *no control* scenario. However, the throughput of the system decreases from 39 per hour in *no control* to 27 per hour in the headway-based control scenario.

We also consider a combination of station-level passenger inflow control and headway-based strategies. We restrict the maximum passenger movement rate at 9.75 passengers per second and we also set the minimum value of D as 70 seconds, as opposed to 60 seconds in the *no control* scenario. Figure 4 shows the time-space diagram for this combined control scenario. The figure illustrates that queuing of trains is completely eliminated under this control strategy and the system throughput increases from 27 per hour in the headway-based control only scenario to 38 trains per hour in the combined control scenario.

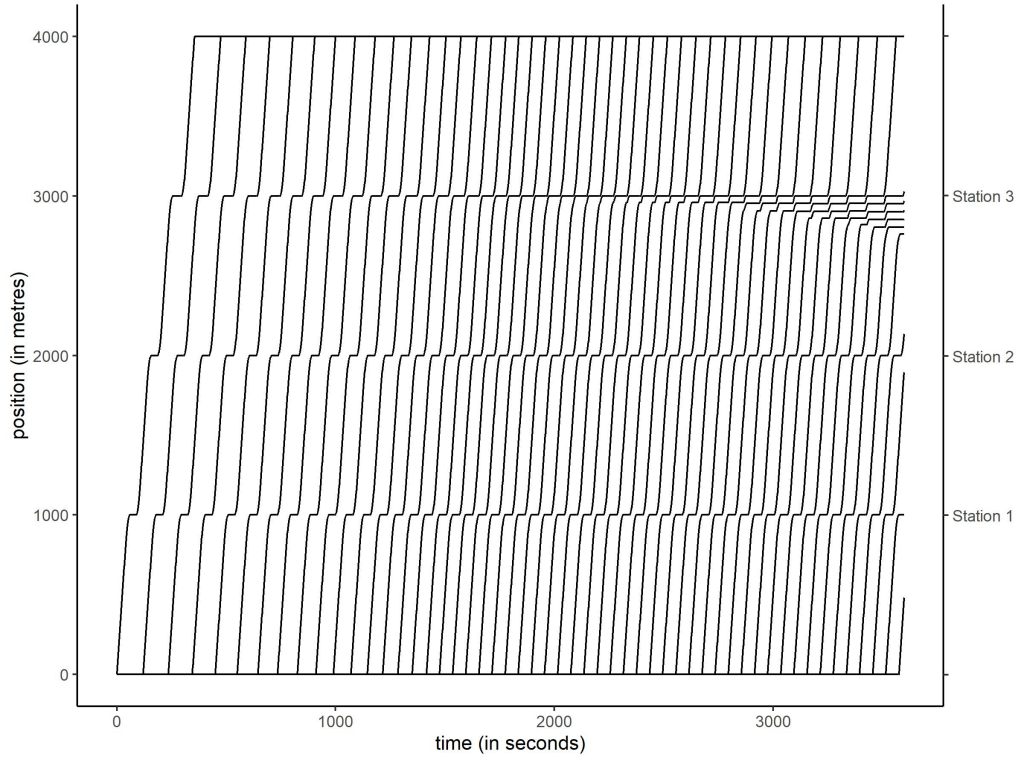


(a) The time-space diagram representing train trajectories.



(b) The train flow versus passenger movement per train diagram.

Figure 1: Train operations under no control scenario.



(a) When maximum passenger movement rate at the bottleneck station is restricted at 9.75 passengers per second.



(b) When maximum passenger movement rate at the bottleneck station is restricted at the optimal level of 9.65 passengers per second.

Figure 2: The time-space diagrams representing train operations under passenger inflow control scenarios.

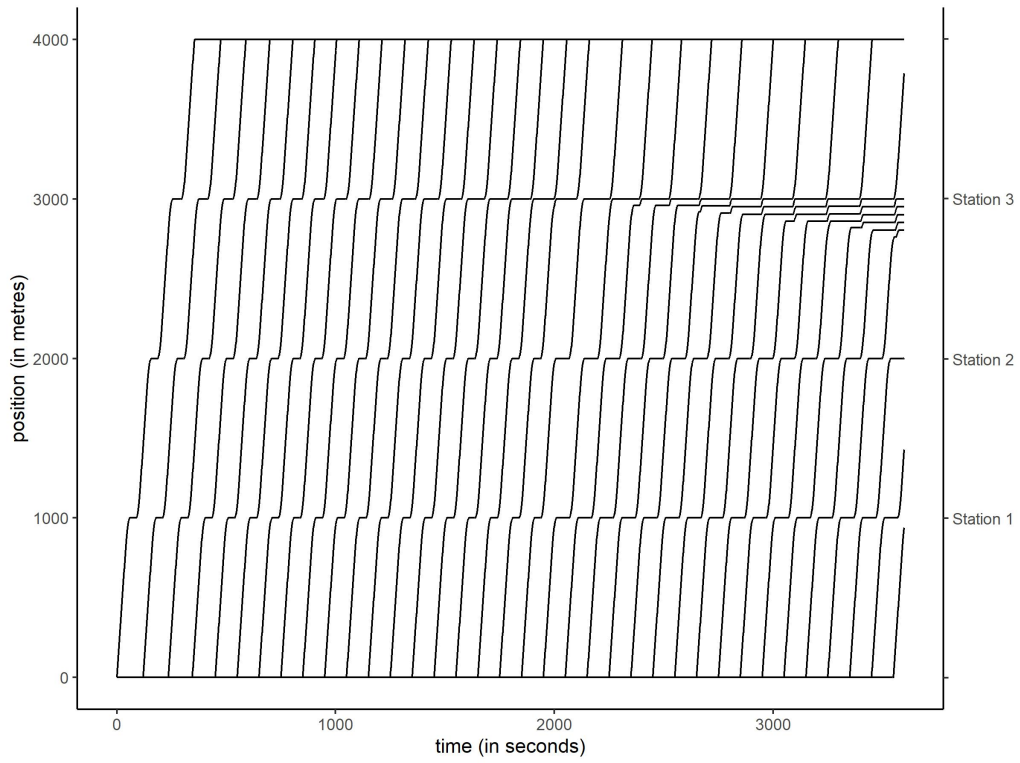


Figure 3: The time-space diagram representing train operations under a headway-based control strategy.

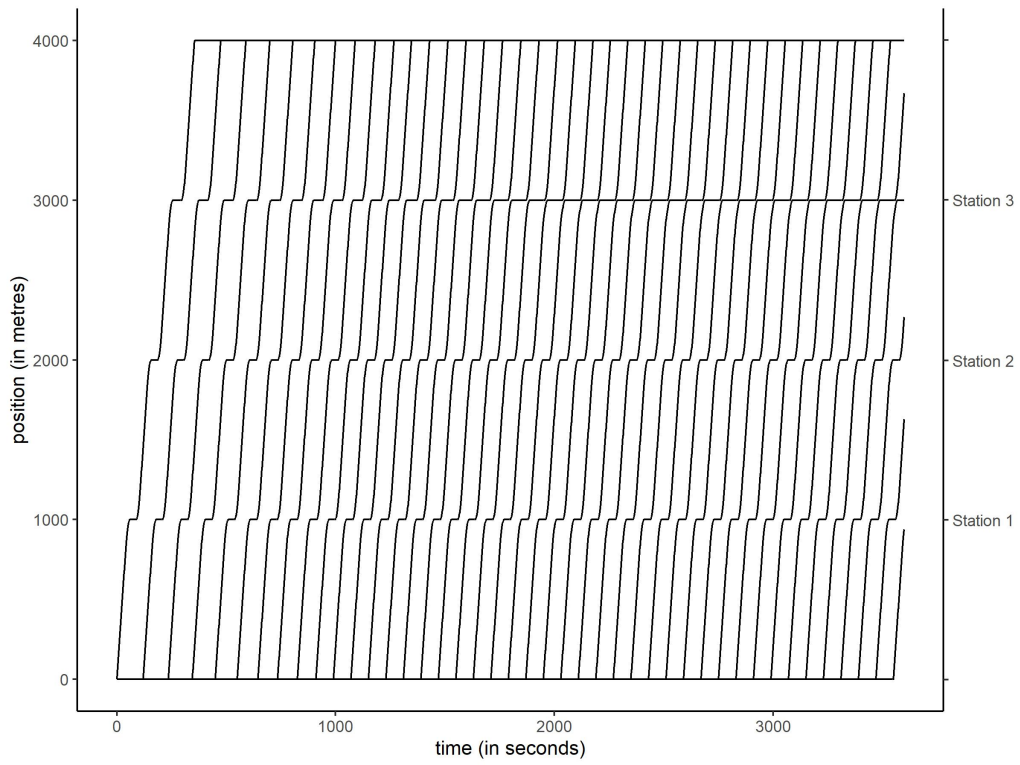


Figure 4: The time-space diagram representing train operations under a combination of passenger inflow control and headway-based control strategies.

The simulation study thus illustrates that ensuring the optimum passenger movement per train at bottleneck stations using station-level controls can be more effective than solely headway-based strategies in reducing congestion-related delays and improving service reliability. This simple exercise also corroborates the findings from some recent studies on bus transit operations, which compare control strategies that combine limiting the number of boarding passengers at stops during peak operations and holding of buses at control stations (headway-control) with those that involve holding of buses only (Delgado et al., 2009, 2012). These studies suggest that the hybrid strategy outperforms the headway-based strategy in improving service reliability by avoiding bus bunching. In the rest of this paper, we show how the bottleneck stations can be identified and how the optimum passenger movements at these stations can be empirically estimated using automated fare collection and train movement data.

3. Model and Data

As discussed in the Introduction section (Section 1), we aim to estimate a *causal relationship* between passenger movements per train and train flows at each station. In other words, the objective of the empirical study is to estimate an equivalent of Figure 1(b) (presented in the simulation exercise in Section 2) for each station using data of Hong Kong MTR. Through these station-level diagrams, we aim to examine whether a unique and optimal passenger volume exists at stations, above which passenger movements negatively affect the train arrival rate.

This section is divided into two subsections. In the first subsection, we discuss the model specification, describe the Bayesian NPIV method in the context of this study and highlight the estimation practicalities. In the second subsection, we describe the data and the relevant variables.

3.1. Methodology

3.1.1. Model Specification

We consider that the average train flow q_{it}^s (that is, inverse of headway) at a station s in the ten-minute interval i on a particular day t is a function of the average number of boarding and alighting movements per train n_{it}^s occurring at the station in that interval:

$$q_{it}^s = S(n_{it}^s) + \omega_{it} + \xi_{it} \quad (3)$$

where ω_{it} represents the unobserved properties of the station-specific operations, such as existing control measures adopted by station staff, ξ_{it} is a idiosyncratic error term representing all random shocks to the dependent variable, and the unknown functional relationship of n_{it}^s with q_{it}^s is denoted by $S(\cdot)$. Based on Figure 1(b), we can expect $S(\cdot)$ to be a step function with different steps representing various regimes of the planned train frequencies. Adopting a parametric specification such as a quadratic function may be too restrictive to capture such non-linearities in the estimated relationship. Therefore, a non-parametric specification of $S(\cdot)$ should be considered to obviate the need for defining its functional form a priori.

In addition, it is worth acknowledging that operators often adopt control measures to restrict passenger movements during peak hours so that the planned dwell times and headway of trains can be maintained. For instance, Transport for London often closes entrances/exits at various stations during peak hours to regulate passenger demand (TfL, 2018). Considering that ω_{it} represents these control measures, we expect a negative correlation between ω_{it} and n_{it}^s and a positive correlation between ω_{it} and q_{it}^s . The unavailability of a measure for ω_{it} may lead to a confounding bias in the estimates of $S(\cdot)$, commonly known as omitted variable bias in the econometrics literature (see Cameron and Trivedi, 2005, for details). In particular, in the absence of a suitable measure or proxy for ω_{it} , an ordinary least squares estimation may underestimate $S(\cdot)$ if $S(\cdot)$ is a linear function (Cameron and Trivedi, 2005). Therefore, we should adopt a nonparametric instrumental variable (NPIV) regression, which not only enables non-parametric specification of $S(\cdot)$ but also addresses any potential confounding biases.

Classical (frequentist) NPIV regression approaches are popular in theoretical econometrics (such as, Newey and Powell, 2003; Horowitz, 2011; Newey, 2013; Chetverikov and Wilhelm, 2017), but they are challenging to apply in practice due to two main reasons. First, tuning parameters to monitor the flexibility of $S(\cdot)$ are often required to be specified by the analyst. Second, standard errors are generally computed using bootstrap, making these methods computationally prohibitive for large datasets. Therefore, we adopt a scalable *Bayesian* NPIV approach, proposed by Wiesenfarth et al. (2014), that can produce a consistent estimate of non-parametric $S(\cdot)$, even if the analyst does not observe ω_{it} . This Bayesian method addresses both challenges of the frequentist estimation because it *learns* tuning parameters related to $S(\cdot)$ during estimation and uncertainty in parameters

estimates is inherently captured by credible intervals (analogous to classical confidence intervals). In addition, it also enables nonparametric specification of the unobserved error component ξ_{it} , precluding the need for making additional assumptions. In Appendix A, we benchmark the performance of the Bayes NPIV estimator against state-of-the-art estimators in a Monte Carlo study and illustrate its superiority in adjusting for endogeneity bias and recovering complex functional forms of $S(\cdot)$.

3.1.2. Bayesian Nonparametric Instrumental Variable Regression

We discuss the Bayesian NPIV approach ([Wiesenfarth et al., 2014](#)) for a model with a single endogenous covariate, that is,

$$q = S(n) + \epsilon_2, \quad n = h(z) + \epsilon_1 \quad (4)$$

Note that ω and ξ are encapsulated in ϵ_2 , and z is an instrument for the endogenous regressor n . The relationship between n and z is represented by an unknown functional form $h(\cdot)$ and ϵ_2 is an idiosyncratic random error term. For the notational simplicity, we drop time-day subscripts. Bayesian NPIV is a control function approach, and assumes the following standard identification restrictions:

$$E(\epsilon_1|z) = 0 \quad \text{and} \quad E(\epsilon_2|\epsilon_1, z) = E(\epsilon_2|\epsilon_1), \quad (5)$$

which yields

$$\begin{aligned} E(q|n, z) &= S(n) + E(\epsilon_2|\epsilon_1, z) = S(n) + E(\epsilon_2|\epsilon_1) \\ &= S(n) + \nu(\epsilon_1), \end{aligned} \quad (6)$$

where $\nu(\epsilon_1)$ is a function of the unobserved error term ϵ_1 . This function is known as the control function.

To satisfy the identification restrictions presented in equation 5, we need an instrumental variable (IV) z . The IV should be (i) exogenous, that is, uncorrelated with ω , ξ , and ϵ_2 ; (ii) relevant, that is, strongly correlated with the endogenous covariate n . Due to the absence of suitable external instruments, we use the lagged level of the endogenous covariate (average passenger movements per train) as an instrument, that is, for average passenger movements observed in the ten-minute interval i on day t , we consider the

observation on the covariate from the same interval i from the previous workday $t - 1$ as its instrument. We argue that the average passenger movements n_{it}^s in the ten-minute interval i on day t is highly correlated with the average passenger movements $n_{i,t-1}^s$ in the same ten-minute interval i on the previous day $t - 1$. This correlation follows from the influence of time-of-the-day on passenger demand. However, these lagged passenger movements $n_{i,t-1}^s$ are exogenous because they do not directly determine the response variable q_{it}^s in equation 3. To justify the relevance of the considered instrument, we present the estimated $h(\cdot)$ in equation 4 in the Results and Discussion Section (Section 4.1).

Conditional on the availability of a valid instrument, Bayesian NPIV can correct for confounding bias. To account for nonlinear effects of continuous covariates, both $S(\cdot)$ and $h(\cdot)$ (refer equation 4) are specified in terms of additive predictors comprising penalised splines. Each of the functions $S(\cdot)$ and $h(\cdot)$ is approximated by a linear combination of suitable B-spline basis functions. The penalised spline approach uses a large enough number of equidistant knots in combination with a penalty to avoid over-fitting. Moreover, the joint distribution of ϵ_1 and ϵ_2 is specified using nonparametric Gaussian Dirichlet process mixture (DPM), which ensures robustness of the model relative to extreme observations. Efficient Markov chain Monte Carlo (MCMC) simulation technique is employed for a fully Bayesian inference. The resulting posterior samples allow us to construct simultaneous credible bands for the non-parametric effects (i.e., $S(\cdot)$ and $h(\cdot)$). Thereby, the possibility of non-normal error distribution is considered and the complete variability is represented by Bayesian NPIV. We now succinctly discuss specifications of the kernel error distribution in Bayesian NPIV.

To allow for a flexible distribution of error terms, the model considers a Gaussian DPM with infinite mixture components, c , in the following hierarchy:

$$\begin{aligned}
(\epsilon_{1i}, \epsilon_{2i}) &\sim \sum_{c=1}^{\infty} \pi_c N(\mu_c, \Sigma_c) \\
(\mu_c, \Sigma_c) &\sim G_0 = N(\mu|\mu_0, \tau_{\Sigma}^{-1}\Sigma) \text{IW}(\Sigma|s_{\Sigma}, S_{\Sigma}) \\
\pi_c &= v_c \left(1 - \sum_{j=1}^{c-1} (1 - \pi_j) \right) = v_c \prod_{j=1}^{c-1} (1 - v_j), \\
c &= 1, 2, \dots \\
v_c &\sim \text{Be}(1, \alpha).
\end{aligned} \tag{7}$$

where μ_c , Σ_c and π_c denote the component-specific means, variances and mixing proportions. The mixture components are assumed to be independent and identically distributed with the base distribution G_0 of the Dirichlet process (DP), where G_0 is given by a normal-inverse-Wishart distribution. The mixture weights are generated in a stick-breaking manner based on a Beta distribution with concentration parameter $\alpha > 0$ of the DP. The concentration parameter α determines the strength of belief in the base distribution G_0 .

3.1.3. Estimation Practicalities

We exclude Gibbs sampler of Bayesian NPIV for brevity, but mainly focus on implementation details and posterior analysis. Interested readers can refer to [Wiesenfarth et al. \(2014\)](#) for derivation of conditional posterior updates. We adapt *BayesIV* and *DPpackage* in R to estimate Bayesian NPIV. We consider 50,000 posterior draws in the estimation, exclude first 15,000 burn-in draws and keep every 10^{th} draw from the remaining draws for the posterior analysis. The point-wise posterior mean is computed by taking average of 3,500 posterior draws. Bayesian simultaneous credible bands are obtained using quantiles of the posterior draws. A simultaneous credible band is defined as the region I_δ such that $P_{S|data}(S \in I_\delta) = 1 - \delta$, that is, the posterior probability that the entire true function $S(\cdot)$ is inside the region given the data equals to $1 - \delta$. The Bayesian simultaneous credible bands are constructed using the point-wise credible intervals derived from the $\delta/2$ and $1 - \delta/2$ quantiles of the posterior samples of $S(\cdot)$ from the MCMC output such that $(1 - \delta)100\%$ of the sampled curves are contained in the credible band. Similar process is used to obtain the credible intervals of $h(\cdot)$.

3.2. Data and Relevant Variables

We use the automatic fare collection (AFC) or data from entry/exit gates at the stations and automatic vehicular location (AVL) or train movement datasets provided by Hong Kong MTR, the urban and suburban rail operator of Hong Kong and a member of the Community of Metros facilitated by the Transport Strategy Centre (TSC) at Imperial College London. The MTR dataset is practical for the present analysis because it is a closed system. All stations in the MTR network are fenced, and thus, the AFC data contain information about all transactions at both the origin and destination stations. The data contain a record for millions of entry/exit transactions corresponding to trips

occurring in the MTR network over the period from January 1, 2019 to March 31, 2019. The AVL data recovered from the signalling system contains a precise record of departure and arrival times of trains at each station in the MTR network for the above mentioned period. We assign passengers to trains by matching automated fare collection data with train movement data using the methodology detailed in [Bansal et al. \(2020\)](#) (an extension to [Hörcher et al. \(2017\)](#)).

In this analysis, we focus on a group of stations on the Kwun Tong Line (green line) that are located in the central business district of Hong Kong. These stations are highlighted in Figure 5.



Figure 5: A part of the MTR network where the line that we study is highlighted in green.

We analyse the trains moving in both downward and upward directions, that is, towards the Whampao and Choi Hung stations respectively. From the results of passenger-train assignment, we calculate train flow and average number of alightings and boardings per train or passenger movements per train for different consecutive ten-minute time intervals throughout a day for each station. Note that train flow in a ten-minute interval for a station is obtained by taking the mean of the inverse of time headway of trains arriving at that station within that interval.

Table 1 presents the summary statistics for ten-minute train flows and average number of boardings and alightings at each station. We note that the four interchange stations – Kowloon Tong, Prince Edward, Mong Kok and Yau Ma Tei – are associated with higher

level of passenger boardings and alightings in either of the two or both directions of train flow as compared to other stations. We provide the observed scatter plots of train flow versus passenger movements per train for the considered stations in Figures 13 and 14 in Appendix B.

Table 1: Summary statistics for variables used in the analysis.

Station	Direction	Variable	Obs.	Min	Max	Mean	Std.Dev
Wong Tai	downward	train flow (tr/10min)	8932	0.35	8.58	3.23	1.00
		passenger movements	8932	8.00	653.00	224.50	87.62
	upward	train flow (tr/10min)	8943	0.33	9.02	3.40	1.06
		passenger movements	8943	4.00	506.0	210.00	67.36
Lok Fu	downward	train flow (tr/10min)	9007	0.35	7.54	3.33	1.03
		passenger movements	9007	3.00	381.00	105.28	41.24
	upward	train flow (tr/10min)	8977	0.32	9.20	3.38	1.07
		passenger movements	8977	3.00	283.50	106.60	40.79
Kowloon Tong	downward	train flow (tr/10min)	9018	0.33	7.74	3.32	1.02
		passenger movements	9018	19.00	2244.00	551.70	222.28
	upward	train flow (tr/10min)	9039	0.38	8.75	3.34	1.05
		passenger movements	9039	10.00	1574.50	519.50	191.67
Shek Kip Mei	downward	train flow (tr/10min)	8946	0.33	8.70	3.34	1.01
		passenger movements	8946	3.00	293.00	88.67	31.99
	upward	train flow (tr/10min)	9008	0.34	9.68	3.35	1.04
		passenger movements	9008	5.33	406.33	86.10	33.19
Prince Edward	downward	train flow (tr/10min)	8959	0.33	8.70	3.34	1.04
		passenger movements	8959	6.00	1523.00	451.50	175.94
	upward	train flow (tr/10min)	8969	0.36	9.49	3.32	1.02
		passenger movements	8969	3.00	1703.50	416.00	158.57
Mong Kok	downward	train flow (tr/10min)	8946	0.34	8.19	3.35	1.01
		passenger movements	8946	10.00	1697.70	544.60	257.76
	upward	train flow (tr/10min)	8970	0.37	10.35	3.02	1.00
		passenger movements	8970	12.00	1595.00	293.40	146.84
Yau Ma Tei	downward	train flow (tr/10min)	9007	0.34	8.25	3.34	1.02
		passenger movements	9007	2.00	398.00	115.53	46.66
	upward	train flow (tr/10min)	8955	0.33	10.79	3.29	1.00
		passenger movements	8955	29.00	2798.00	524.70	274.03

*Obs.: Number of observations, Std. Dev.: Standard Deviation, tr/10min: trains per ten minutes

**Passenger movements represent average no. of boardings and alightings per train

4. Results and Discussion

This section is divided into four subsections. In the first subsection, we compare results from our IV-based estimator with those from a non-IV estimator. The non-IV estimator is a counterpart of the Bayesian NPIV, which does not address confounding bias (that is, $z = n; \epsilon_1 = 0; h$: identity function in Equation 4). In the next subsection, we discuss the estimated kernel error distributions to illustrate the importance of the non-parametric DPM specification. We discuss the relevance of our instruments in the penultimate subsection. We conclude this section by describing Bayesian NPIV results in

detail and discussing how we identify the optimal passenger movement at the bottleneck stations.

4.1. Comparison of IV-based and non-IV-based estimators

We compare the estimates of $S(\cdot)$ in equation 4 (second-stage), which we obtain using the Bayesian NPIV, and its non-IV-based counterpart, for Prince Edward Station for train flows in both downward and upward direction as shown in Figures 6 and 7.

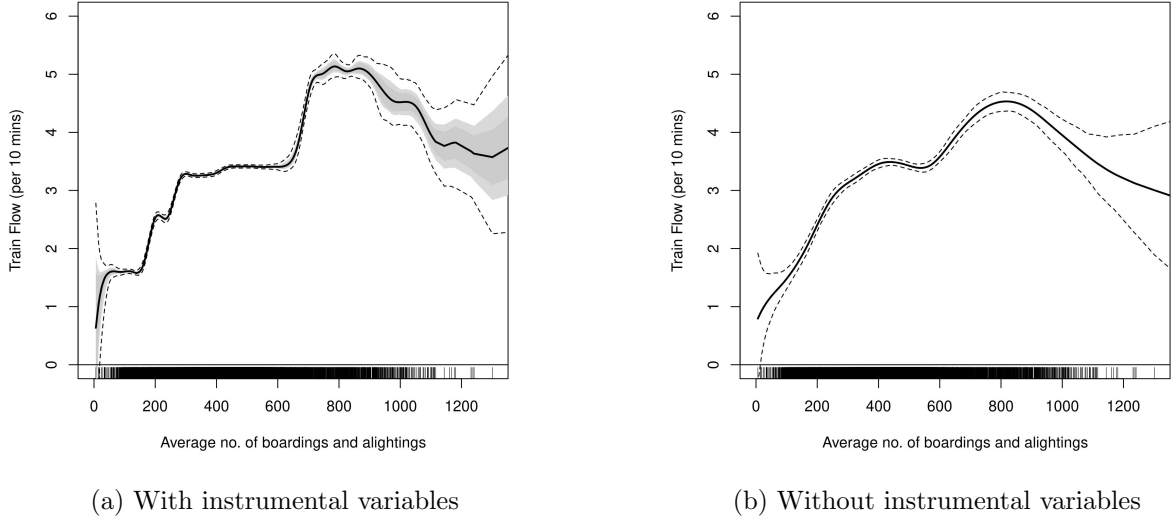


Figure 6: Train Flow (per 10 minutes) in downward direction versus Average number of boardings and alightings (in 10 minutes) at Prince Edward Station.

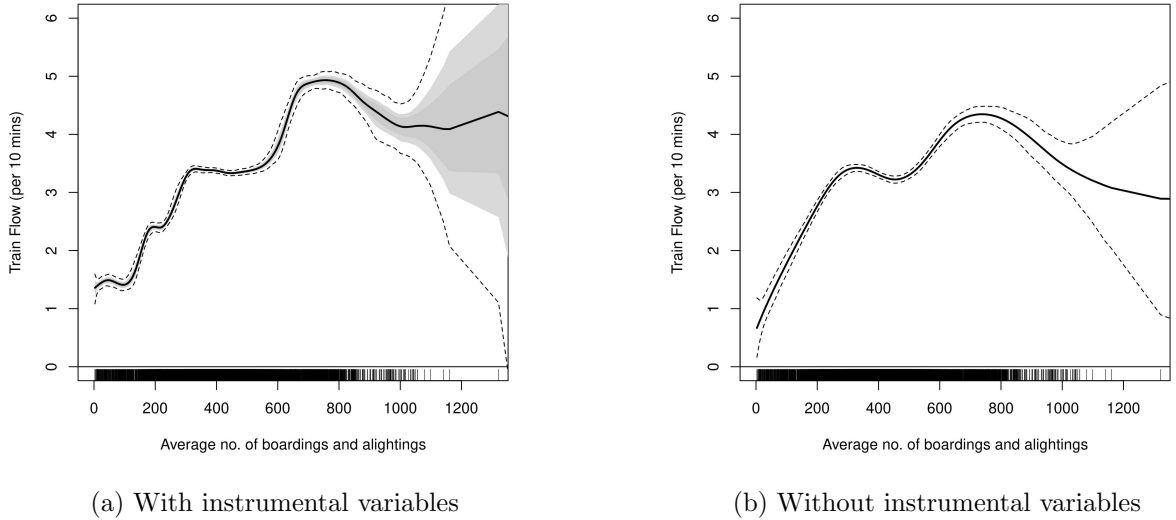


Figure 7: Train Flow (per 10 minutes) in upward direction vs Average number of boardings and alightings (in 10 minutes) at Prince Edward Station.

Both figures suggest that IV-based estimate of $S(\cdot)$ is as efficient as its non-IV counterpart, that is, both have similar and tight credible bands for the domain of passenger movements where we have sufficient number of observations (note that the density of the tick marks on the X-axis represents the number of observations).

However, the maximum train flow is slightly underestimated by the non-IV estimator in both figures. As discussed in Section 3.1.1, such bias is expected in the non-IV-based estimate due to the absence of suitable control for unobserved characteristics of metro operations. Moreover, the multi-step function estimated from the IV-based method is more plausible as it could detect multiple regimes of the planned train frequencies, instead of binary regimes illustrated by non-IV estimates (see [Travel China Guide, 2019](#), for time-of-day frequency of the Kwun Tong Line). The results indicate that the endogeneity bias is less severe in our case, however, it may be more pronounced in other similar empirical studies depending upon their data generating processes. The advantages of adopting NPIV would be even more apparent in presence of large endogeneity biases.

4.2. Distribution of Errors

Figure 8 shows the contour plot of the joint distribution of errors from the second stage (ϵ_2) and the first stage (ϵ_1) for both directions of train flows at Prince Edward Station. From these figures, we observe the joint error distribution is bi-modal.

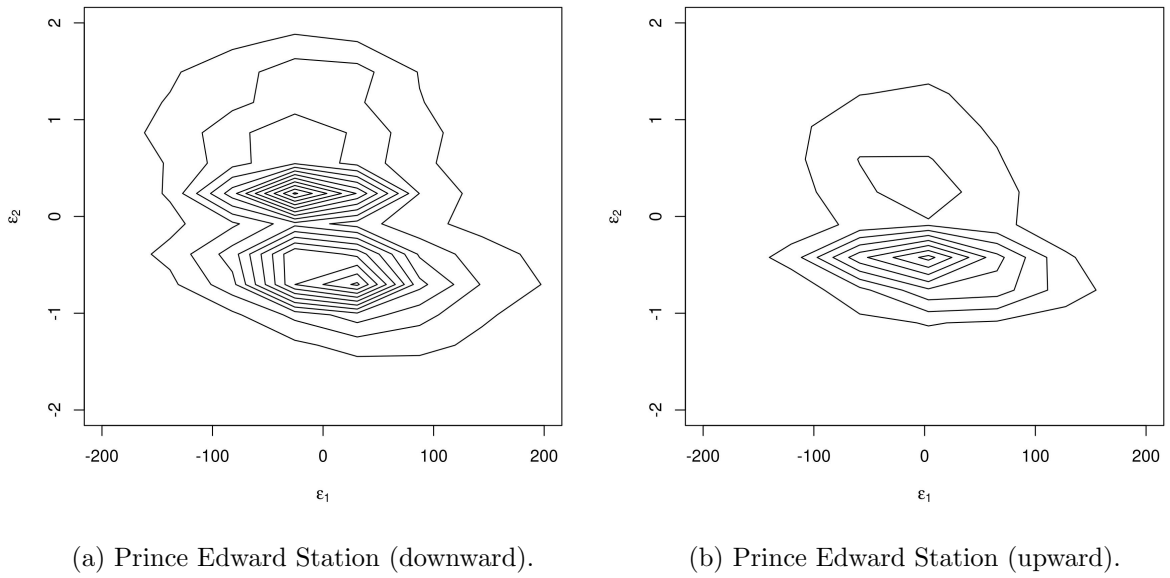


Figure 8: Distribution of errors.

The results suggest that the estimates of $S(\cdot)$ from traditional econometric methods could have poor finite sample properties because they generally assume uni-modal symmetric and thin-tailed Gaussian error distributions. The adopted Bayesian NPIV method addresses all these potential challenges by allowing for a flexible distribution of errors, instead of assuming a restrictive parametric error distribution.

4.3. Relevance of Instruments

Figure 9 illustrates the results (that is, the estimated $h(\cdot)$) from regression of the endogenous covariate over the chosen instrument for the two directions of train flows at Prince Edward Station.

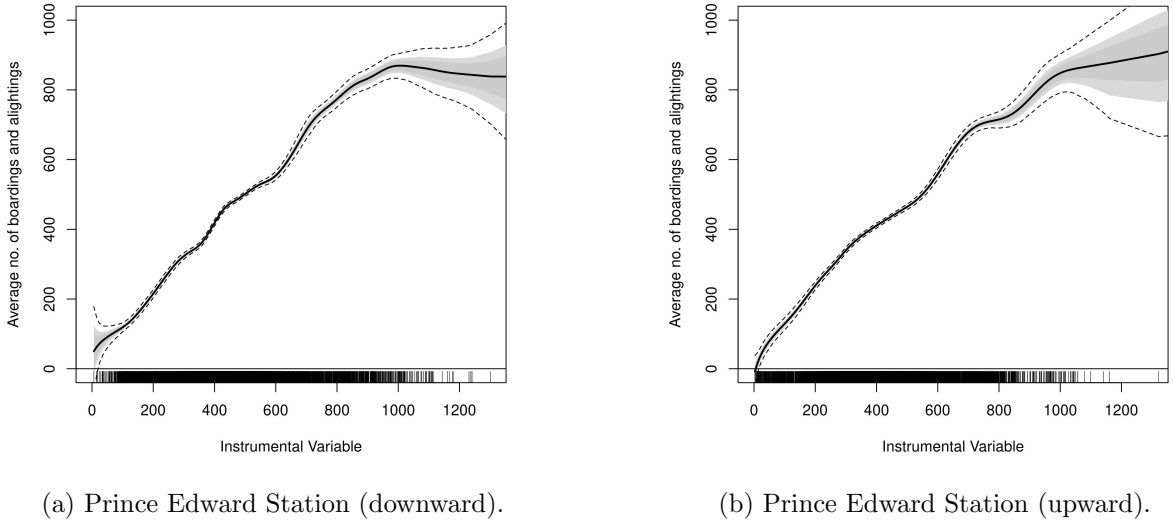


Figure 9: Strength of instruments used in this analysis.

From these figures, we notice a strong correlation between the instrument and the endogenous covariate. These figures provide supporting evidence that the selected instruments satisfies the relevance condition. For other stations, we observe similar patterns of correlation between the instrument (that is, passenger movements per train in a given time-of-the-day on the previous workday) and the endogenous covariate, but we omit them here for brevity.

4.4. Bottlenecks and station-level optimal passenger movements

Figures 10 and 11 show the estimated train flow versus passenger movement per train curves (that is, the estimated $S(\cdot)$ in the second stage) for all stations that are highlighted in Figure 5 for downward and upward directions respectively. We observe

that all the estimated curves are nearly concave, but the associated credible bands in the backward bending region are very wide for all stations, except for Prince Edward Station in the downward direction and Kowloon Tong Station, Mong Kok Station, Prince Edward Station and Yau Ma Tei Station in the upward direction (see Figures 10c, 11c, 11e, 11f, 11g). However, the statistical significance of the backward bending part is apparent in a short range of passenger movements at these stations. Thus, these plots provide empirical evidence to support the existence of a unique and optimal passenger volume, above which passenger movements negatively affect the train arrival rate.

The stations with statistically significant backward bending act as active bottlenecks in the associated direction of train flow along Kwun Tong Line in the MTR network. In the downward direction, the optimal number of passenger boardings and alightings at Prince Edward Station is around nine hundred passengers. In the upward direction, the optimal number of passenger boardings and alightings is around nine hundred passengers at Kowloon Tong Station, around eight hundred passengers at Prince Edward Station, around seven hundred passengers at Mong Kok Station, and around eleven hundred passengers at Yau Mai Tei Station. The corresponding maximum train inflow at all the bottleneck stations is around five trains per ten minutes, that is, the estimated minimum headway between trains is around two minutes. The estimated minimum headway value in both directions is consistent with the planned minimum peak headway of 2.1 minutes (Travel China Guide, 2019). Table 2 summarises these results. Thus, the application of the NPIV approach allows us to adjust for any confounding bias and recover the scheduled peak headway.

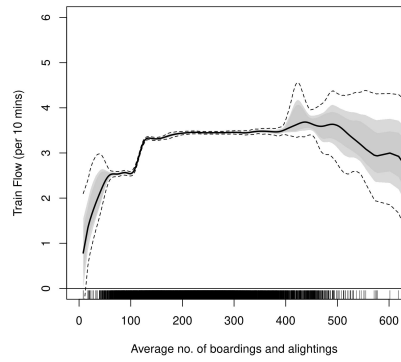
The large credible intervals in the backward bending part of the estimated $S(\cdot)$ at all other stations implies that there may be only a handful of instances of the delay propagation from bottlenecks to these stations due to in-place control measures and relatively lower operating frequency of the MTR services. Thus, the estimated relationship between train flow and passenger movements and optimal/critical passenger movements are not universal, rather they depend upon the characteristics of the metro network such as metro demand, frequency, and spacing between stations, station design among many others.

Table 2: Summary of results.

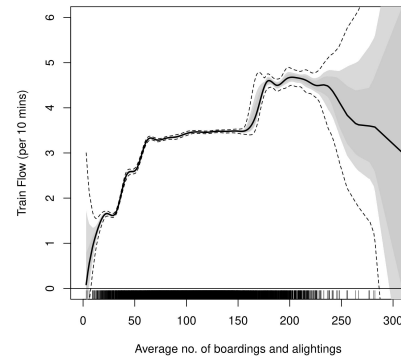
Identified Bottleneck Station	Direction of Flow	Optimum passenger movements	Scheduled peak headway
Prince Edward	downward	~ 900 pax per train	~ 2 minutes
Kowloon Tong	upward	~ 900 pax per train	~ 2 minutes
Mong Kok	upward	~ 700 pax per train	~ 2 minutes
Prince Edward	upward	~ 800 pax per train	~ 2 minutes
Yau Ma Tei	upward	~ 1100 pax per train	~ 2 minutes

To show the relevance of the estimated optimum passenger movement from a conceptual perspective and illustrate its importance in devising control strategies, we briefly discuss the analogous concept of *capacity* and *critical density* from traffic flow theory. Understanding traffic capacity and the corresponding critical density at the link- or network-level has been the main focus in the modelling of traffic flow (Srivastava and Geroliminis, 2013; Siebel et al., 2009; Laval and Daganzo, 2006; Loder et al., 2019; Geroliminis and Daganzo, 2008; Daganzo and Geroliminis, 2008). This is because the capacity may be insufficient for the peak-hour demand and the system may transition from a free-flow state to a congested state. With the increase in the number of vehicles in the system, travel production decreases in the congested state but increases in the free-flow state. Traffic control strategies like ramp metering and congestion pricing aim to regulate the demand to maximise the link- or network-level travel production (Papageorgiou et al., 2003; Small et al., 2007). The existence of a well-defined fundamental diagram between traffic flow and traffic density and the corresponding estimates of traffic capacity and critical density over which productivity of the system falls, have been crucial inputs in the development of such traffic control strategies.

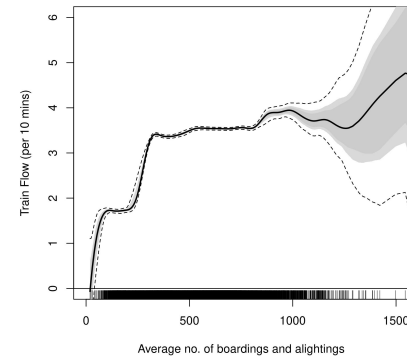
Similar to the fundamental diagram in traffic flow theory, we illustrate the existence of a well-defined relationship between passenger movements and train flow at a station in metros. Furthermore, we find that there also exists a unique critical level of passenger movements, over which the throughput of the metro line decreases. These estimates could be crucial inputs in the design of passenger inflow control strategies that are similar to vehicular control strategies in road traffic.



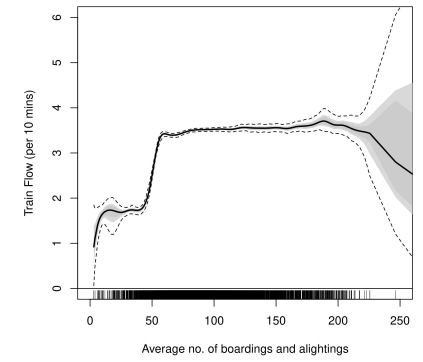
(a) Wong Tai Sin Station



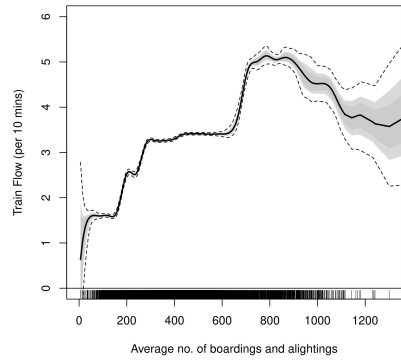
(b) Lok Fu Station



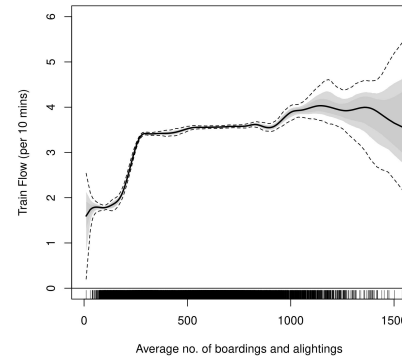
(c) Kowloon Tong Station



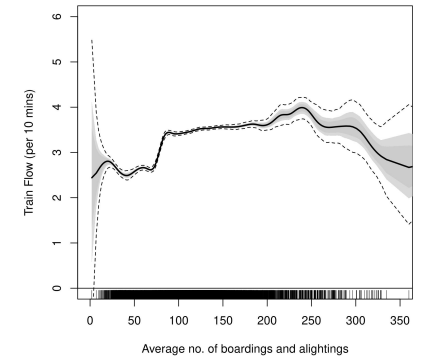
(d) Shek Kip Mei Station



(e) Prince Edward Station

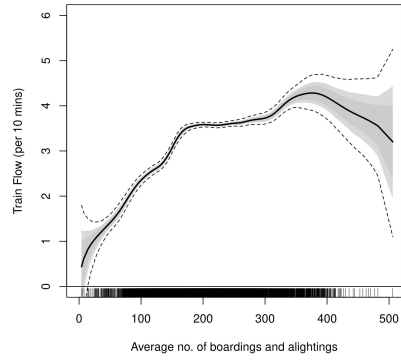


(f) Mong Kok Station

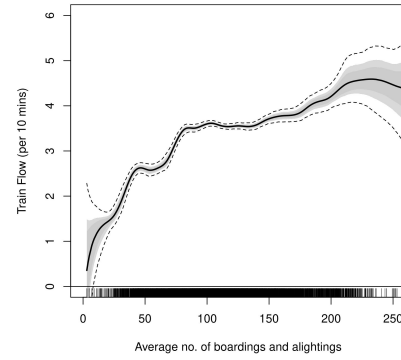


(g) Yau Ma Tei station

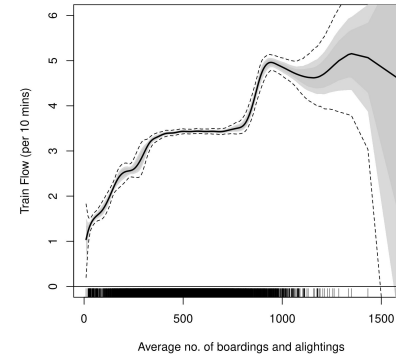
Figure 10: Non-parametric Instrumental Variables based estimation results for train movements in the downward direction along the Kwun Tong Line.



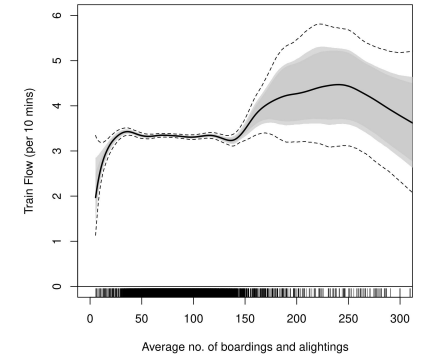
(a) Wong Tai Sin Station



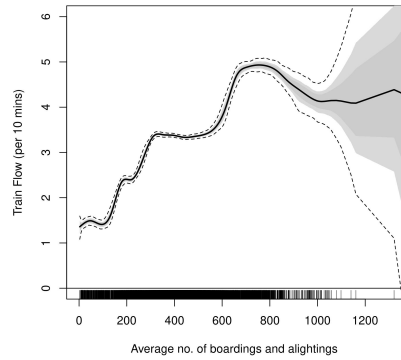
(b) Lok Fu Station



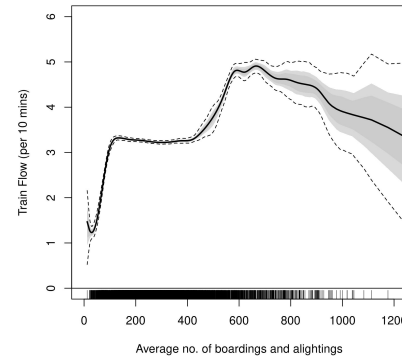
(c) Kowloon Tong Station



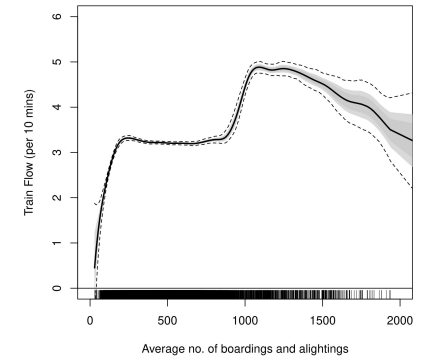
(d) Shek Kip Mei Station



(e) Prince Edward Station



(f) Mong Kok Station



(g) Yau Ma Tei station

Figure 11: Non-parametric Instrumental Variables based estimation results for train movements in the upward direction along the Kwun Tong Line.

5. Conclusions and Relevance

This paper provides the first station-level analysis of congestion in a metro network by estimating a causal relationship between passenger movement per train and train flow. We use automated fare collection and train movement data from Hong Kong MTR and adopt a data-driven Bayesian non-parametric instrumental variable method to address potential confounding biases in the estimated relationship. This analysis could help metro operators to identify bottleneck stations in the network. Furthermore, optimum passenger movements and corresponding train frequencies are also obtained as a by-product of the estimation.

The short-term prediction of subway passenger demand has received significant attention in recent years (Ding et al., 2016; Ma et al., 2018). This study enhances the value of short-term demand prediction by estimating its causal impact on train frequencies. Understanding the dynamics of passenger movements and train frequencies, along with estimates of optimum passenger movement, can help in designing strategies to control passenger movements and minimise delays. Such control strategies may involve i) adopting platform management practices such as reducing escalator capacity, ii) deployment of staff resources to regulate the entry of passengers into bottleneck stations, and iii) pricing policies. Another strategy could be *ramp metering*² of passengers entering stations to increase overall system throughput. Daganzo (2005, 2007) suggest such strategies in the context of vehicular traffic control in urban networks.

We note that metro operators around the world presently implement such strategies based on their day-to-day experience of congestion patterns at various stations. For instance, Transport for London implements different types of station control measures such as avoid train dwelling at particular stations during a specific time of the day, individual platform closures, and closures of gate lines and entrances (TfL, 2018). The findings of this study could assist metro operators in improving these control strategies in a data-driven manner.

It is worth noting that the above-discussed strategies rely on controlling passenger boarding movements, but the estimated relationship includes both passenger boarding

²A ramp meter is a basic traffic light device together with a signal controller, that are used to regulate the flow of vehicular traffic entering freeways according to current traffic conditions. Ramp metering systems have proved to be successful in decreasing traffic congestion on freeways. Similar strategies are being sought after by metro operators to regulate passenger demand in future.

and alighting movements. This disparity does not restrict the application of the empirical results in practice because metro operators can use short-term demand prediction models to forecast the number of alighting and boarding movements at any station. Subsequently, they can adopt station-level control measures to regulate the number of boarding movements such that the instantaneous sum of boarding and alighting movements remains optimum. Developing and testing such control measures using real data is an important avenue for future research. Another interesting area of future research could be to explore the potential of fundamental diagrams in the long-run to understand the level of operational service and guide improvements in the metro network.

Acknowledgement

Authors are grateful to Hong Kong MTR for providing data used in the empirical study. They are also thankful to Manuel Wiesenfarth for helpful email conversations and support in figuring out the implementation details of the adopted method. The authors are also grateful to Alexander Barron from the Transport Strategy Centre at Imperial College for his insightful suggestions on the manuscript.

References

- Bansal, P., Hörcher, D. and Graham, D. J. (2020), ‘A dynamic choice model with heterogeneous decision rules: Application in estimating the user cost of rail crowding’, *arXiv preprint arXiv:2007.03682* .
- Cameron, A. C. and Trivedi, P. K. (2005), *Microeconometrics: methods and applications*, Cambridge university press.
- Carey, M. and Kwieciński, A. (1994), ‘Stochastic approximation to the effects of headways on knock-on delays of trains’, *Transportation Research Part B: Methodological* **28**(4), 251–267.
- Chetverikov, D. and Wilhelm, D. (2017), ‘Nonparametric instrumental variables estimation under monotonicity’, *Econometrica* **85**(4), 1303–1320.
- Daganzo, C. F. (1997), *Fundamentals of transportation and traffic operations*, Vol. 30, Pergamon Oxford.
- Daganzo, C. F. (2005), ‘Improving city mobility through gridlock control: an approach and some ideas’.
- Daganzo, C. F. (2007), ‘Urban gridlock: Macroscopic modeling and mitigation approaches’, *Transportation Research Part B: Methodological* **41**(1), 49–62.
- Daganzo, C. F. (2009), ‘A headway-based approach to eliminate bus bunching: Systematic analysis and comparisons’, *Transportation Research Part B: Methodological* **43**(10), 913–921.
- Daganzo, C. F. and Geroliminis, N. (2008), ‘An analytical approximation for the macroscopic fundamental diagram of urban traffic’, *Transportation Research Part B: Methodological* **42**(9), 771–781.
- Delgado, F., Munoz, J. C. and Giesen, R. (2012), ‘How much can holding and/or limiting boarding improve transit performance?’, *Transportation Research Part B: Methodological* **46**(9), 1202–1217.
- Delgado, F., Munoz, J. C., Giesen, R. and Cipriano, A. (2009), ‘Real-time control of

- buses in a transit corridor based on vehicle holding and boarding limits’, *Transportation Research Record* **2090**(1), 59–67.
- Ding, C., Wang, D., Ma, X. and Li, H. (2016), ‘Predicting short-term subway ridership and prioritizing its influential factors using gradient boosting decision trees’, *Sustainability* **8**(11), 1100.
- Geroliminis, N. and Daganzo, C. F. (2008), ‘Existence of urban-scale macroscopic fundamental diagrams: Some experimental findings’, *Transportation Research Part B: Methodological* **42**(9), 759–770.
- Gill, D. C. (1994), ‘Railway signalling system’. US Patent 5,366,183.
- Guo, J., Jia, L., Qin, Y. and Zhou, H. (2015), ‘Cooperative passenger inflow control in urban mass transit network with constraint on capacity of station’, *Discrete Dynamics in Nature and Society* **2015**.
- Hong Kong MTR (2019), ‘Investing for the future’.
URL: <https://tinyurl.com/y459kjnæ>
- Horowitz, J. L. (2011), ‘Applied nonparametric instrumental variables estimation’, *Econometrica* **79**(2), 347–394.
- Hörcher, D., Graham, D. J. and Anderson, R. J. (2017), ‘Crowding cost estimation with large scale smart card and vehicle location data’, *Transportation Research Part B: Methodological* **95**, 105–125.
- Independent (2017), ‘Tube passengers wasted 400,000 hours in 2016 because of overcrowding delays’, *Independent, UK* .
URL: <http://tiny.cc/0mvlsz>
- Jiang, Z., Fan, W., Liu, W., Zhu, B. and Gu, J. (2018), ‘Reinforcement learning approach for coordinated passenger inflow control of urban rail transit in peak hours’, *Transportation Research Part C: Emerging Technologies* **88**, 1–16.
- Keiji, K., Naohiko, H. and Shigeru, M. (2015), ‘Simulation analysis of train operation to recover knock-on delay under high-frequency intervals’, *Case Studies on Transport Policy* **3**(1), 92–98.

- Laval, J. A. and Daganzo, C. F. (2006), ‘Lane-changing in traffic streams’, *Transportation Research Part B: Methodological* **40**(3), 251–264.
- Li, K. P., Gao, Z. Y. and Ning, B. (2005), ‘Cellular automaton model for railway traffic’, *Journal of Computational Physics* **209**(1), 179–192.
- Loder, A., Ambühl, L., Menendez, M. and Axhausen, K. W. (2019), ‘Understanding traffic capacity of urban networks’, *Scientific reports* **9**(1), 1–10.
- London Assembly (2019), ‘Delays on the london underground caused by overcrowding’, *Questions to the Mayor, Mayor of London* .
URL: <http://tiny.cc/4mvlasz>
- Ma, X., Zhang, J., Du, B., Ding, C. and Sun, L. (2018), ‘Parallel architecture of convolutional bi-directional lstm neural networks for network-wide metro ridership prediction’, *IEEE Transactions on Intelligent Transportation Systems* **20**(6), 2278–2288.
- Meng, Q. and Weng, J. (2011), ‘An improved cellular automata model for heterogeneous work zone traffic’, *Transportation research part C: emerging technologies* **19**(6), 1263–1275.
- Nagel, K. and Schreckenberg, M. (1992), ‘A cellular automaton model for freeway traffic’, *Journal de physique I* **2**(12), 2221–2229.
- Newey, W. K. (2013), ‘Nonparametric instrumental variables estimation’, *American Economic Review* **103**(3), 550–556.
- Newey, W. K. and Powell, J. L. (2003), ‘Instrumental variables estimation of nonparametric models’, *Econometrica* **71**(5), 1565–1578.
- Ning, B., Xun, J., Gao, S. and Zhang, L. (2014), ‘An integrated control model for headway regulation and energy saving in urban rail transit’, *IEEE Transactions on Intelligent Transportation Systems* **16**(3), 1469–1478.
- Papageorgiou, M., Diakaki, C., Dinopoulou, V., Kotsialos, A. and Wang, Y. (2003), ‘Review of road traffic control strategies’, *Proceedings of the IEEE* **91**(12), 2043–2067.
- Seo, T., Wada, K. and Fukuda, D. (2017), A macroscopic and dynamic model of urban

- rail transit with delay and congestion, in ‘96th Annual Meeting of the Transportation Research Board’.
- Shi, J., Yang, L., Yang, J. and Gao, Z. (2018), ‘Service-oriented train timetabling with collaborative passenger flow control on an oversaturated metro line: An integer linear optimization approach’, *Transportation Research Part B: Methodological* **110**, 26–59.
- Siebel, F., Mauser, W., Moutari, S. and Rascle, M. (2009), ‘Balanced vehicular traffic at a bottleneck’, *Mathematical and Computer Modelling* **49**(3-4), 689–702.
- Small, K. A., Verhoef, E. T. and Lindsey, R. (2007), *The economics of urban transportation*, Routledge.
- Spyropoulou, I. (2007), ‘Modelling a signal controlled traffic stream using cellular automata’, *Transportation Research Part C: Emerging Technologies* **15**(3), 175–190.
- Srivastava, A. and Geroliminis, N. (2013), ‘Empirical observations of capacity drop in freeway merges with ramp control and integration in a first-order model’, *Transportation Research Part C: Emerging Technologies* **30**, 161–177.
- Takeuchi, H., Goodman, C. and Sone, S. (2003), ‘Moving block signalling dynamics: performance measures and re-starting queued electric trains’, *IEE Proceedings-electric power applications* **150**(4), 483–492.
- TfL (2018), ‘Transport for london customer service and operational performance report’, *Transport for London* .
URL: <http://tiny.cc/8ywlsz>
- Tirachini, A., Hensher, D. A. and Rose, J. M. (2013), ‘Crowding in public transport systems: effects on users, operation and implications for the estimation of demand’, *Transportation research part A: policy and practice* **53**, 36–52.
- Travel China Guide (2019), ‘Kwun Tong Line, Hong Kong MTR’.
URL: <https://tinyurl.com/y45467z4>
- Wada, K., Akamatsu, T. and Osawa, M. (2012), A control strategy to prevent propagating delays in high-frequency railway systems, in ‘The 1st European Symposium on Quantitative Methods in Transportation Systems’.

- Wang, X., Wu, J., Yang, X., Guo, X., Yin, H. and Sun, H. (2020), ‘Multistation coordinated and dynamic passenger inflow control for a metro line’, *IET Intelligent Transport Systems* **14**(9), 1068–1078.
- Wiesenfarth, M., Hisgen, C. M., Kneib, T. and Cadarso-Suarez, C. (2014), ‘Bayesian non-parametric instrumental variables regression based on penalized splines and dirichlet process mixtures’, *Journal of Business and Economic Statistics* **32**(3), 468–482.
- Xun, J., Ning, B., Li, K.-p. and Zhang, W.-b. (2013), ‘The impact of end-to-end communication delay on railway traffic flow using cellular automata model’, *Transportation Research Part C: Emerging Technologies* **35**, 127–140.
- Yan, X., Cheng-Xun, C., Ming-Hua, L. and Jin-Long, L. (2012), ‘Modeling and simulation for urban rail traffic problem based on cellular automata’, *Communications in Theoretical Physics* **58**(6), 847.
- Yinping, F., Ziyou, G. and Keping, L. (2008), ‘Modeling study for tracking operation of subway trains based on cellular automata’, *Journal of Transportation Systems Engineering and Information Technology* **8**(4), 89–95.
- Yuan, F., Sun, H., Kang, L. and Wu, J. (2020), ‘Passenger flow control strategies for urban rail transit networks’, *Applied Mathematical Modelling* **82**, 168–188.
- Zhang, J. and Wada, K. (2019), Fundamental diagram of urban rail transit: An empirical investigation by boston’s subway data, in ‘8th Symposium of the European Association for Research in Transportation’.
- Zou, Q., Yao, X., Zhao, P., Dou, F. and Yang, T. (2018), ‘Managing recurrent congestion of subway network in peak hours with station inflow control’, *Journal of Advanced Transportation* **2018**.

Appendix A

We succinctly demonstrate the challenges of functional form mis-specification and endogeneity in an instance of a Monte Carlo study. We benchmark the Bayesian NPIV method against state-of-the-art estimators to illustrate how this method is robust to both issues. In the data generating process (DGP), we consider a concave regression function, that is, a fourth degree polynomial specification but our conclusions are applicable for a more complex specification.

We use a sample of 10000 observations, with the following DGP:

$$\begin{aligned}y &= -40x^4 + 40x^3 + 30w^4 + \epsilon_2 \\x &= 3.5z + 2.1w + \epsilon_1\end{aligned}\tag{8}$$

where z and w are independent and uniformly distributed on $[0,1]$. ϵ_1 and ϵ_2 are independent and identically distributed draws from the $N[0,0.5]$ distribution. The variables y represents the primary response variable, x denotes the endogenous covariate and z represents the instrumental variable. The variable w captures the unobserved effects in the model, that is, we assume that the analyst is ignorant of its presence in the true data generating process for the dependent variable. We thus introduce one possible source of confounding into the model: a positive correlation between the unobserved effect w and the endogenous covariate x .

We note that the model set-up is similar in structure to equation 4, that is:

$$\begin{aligned}y &= s(x) + \epsilon_2 \\x &= h(z) + \epsilon_1\end{aligned}\tag{9}$$

We apply four different estimators to estimate the curve $s(x)$:

1. A two-stage least square (2SLS) estimator with a quadratic specification for $s(x)$.³
2. A two-stage least square (2SLS) estimator with the true specification for $s(x)$.
3. A Bayesian non-parametric estimator without instrumental variables (Bayes NP).
4. A Bayesian non-parametric estimator with instrumental variables (Bayes NPIV).

³Instead of a traditionally-used linear specification, we choose quadratic specification in 2SLS because the scatter plot of the data would intuitively suggest the analyst to use such functional form of $s(x)$.

In the latter two approaches, we take 40000 Posterior draws to ensure stationarity of Markov chains. For the posterior analysis, the initial 10000 draws were discarded for burn-in and every 40th draw of the subsequent 30,000 draws was used for posterior inference. Figure 12 overlays the estimated $s(x)$ from the four approaches and true $s(x)$.

We note that a 2SLS estimator with the true specification for $s(x)$ is able adjust for the endogeneity bias and could produce an unbiased estimate of $s(x)$. However, in practice, it is infeasible for the analyst to know the correct functional form specification a priori. A functional form mis-specification can produce a highly biased estimate of $s(x)$, as shown by the estimated $s(x)$ using the 2SLS estimator with a quadratic specification for $s(x)$. This exercise thus illustrates the importance of adopting a fully flexible non-parametric specification for $s(x)$ in a relationship.

However, in the presence of endogeneity, a traditional non-parametric estimator may fail to produce an unbiased estimate of $s(x)$. From Figure 12, we note that the curve produced by the Bayes NP is highly biased. Adopting an estimator such as the Bayes NPIV allows to adjust for the endogeneity bias and produce an unbiased estimate of the curve $s(x)$.

In summary, this Monte Carlo exercise shows that the Bayes NPIV estimator, the one adopted in this study, outperforms other parametric and non-parametric approaches as it allows for a fully flexible functional form specification and controls for any potential confounding bias.

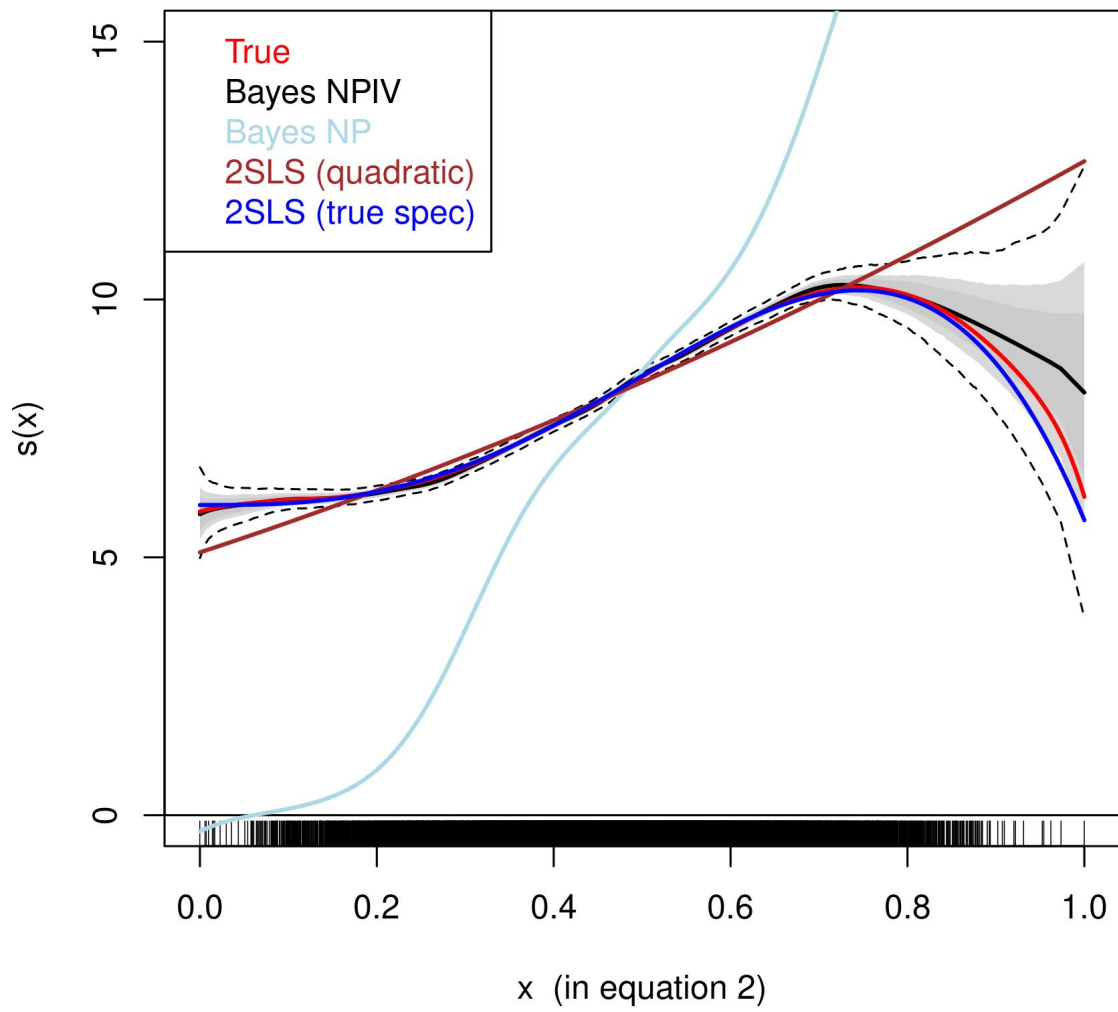
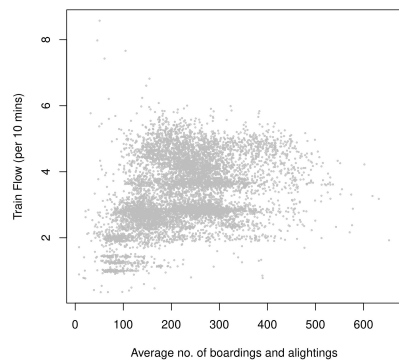
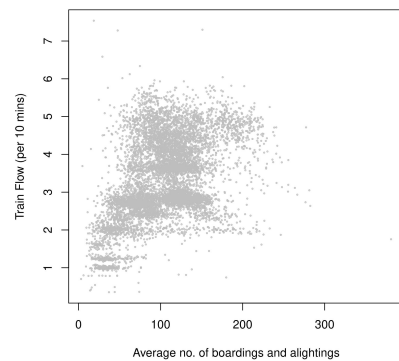


Figure 12: Comparison of different estimators in the Monte Carlo study.

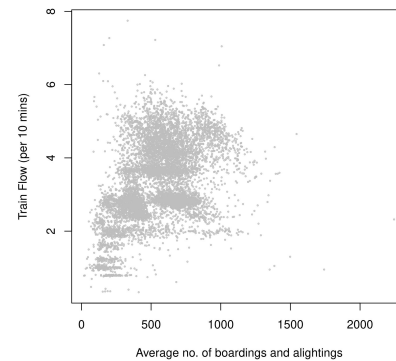
Appendix B



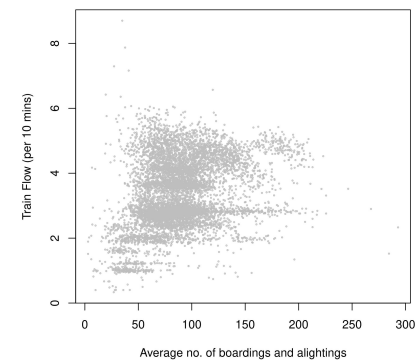
(a) Wong Tai Sin Station



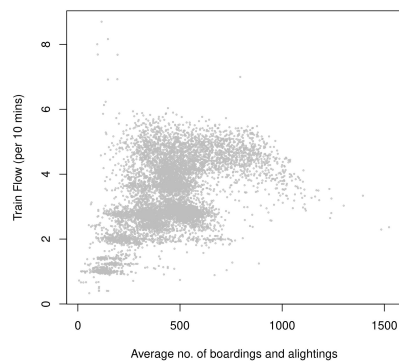
(b) Lok Fu Station



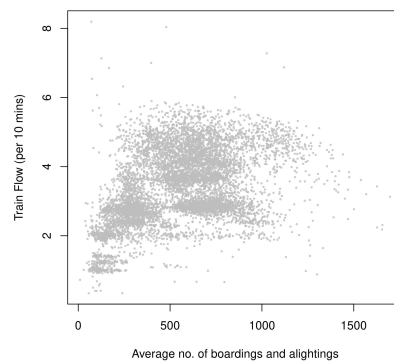
(c) Kowloon Tong Station



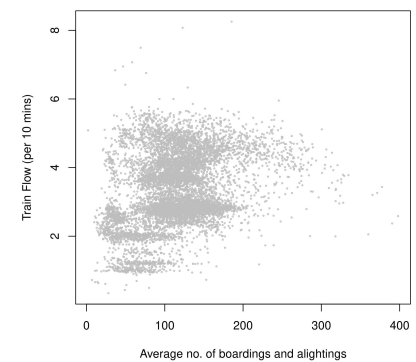
(d) Shek Kip Mei Station



(e) Prince Edward Station

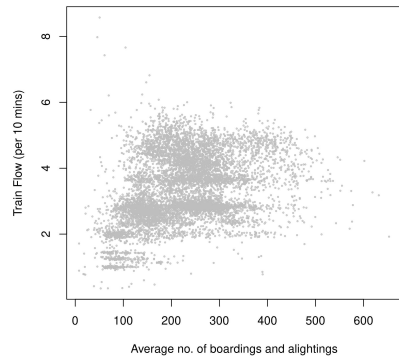


(f) Mong Kok Station

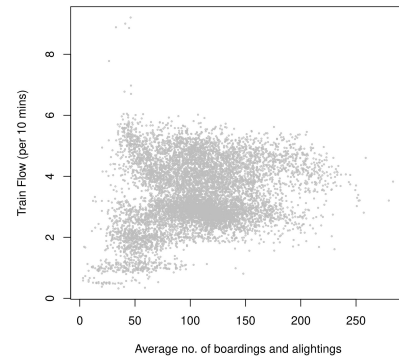


(g) Yau Ma Tei station

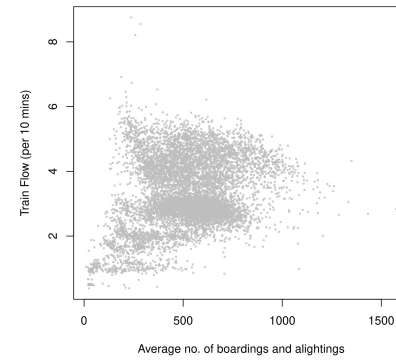
Figure 13: Variation of observed train flow in the downward direction over passenger movements for the stations highlighted in Figure 5.



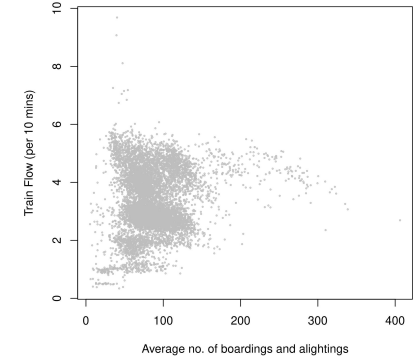
(a) Wong Tai Sin Station



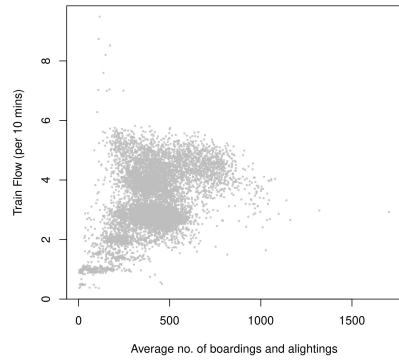
(b) Lok Fu Station



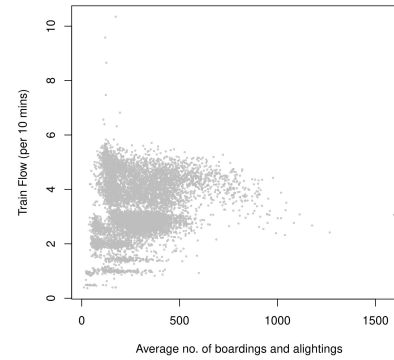
(c) Kowloon Tong Station



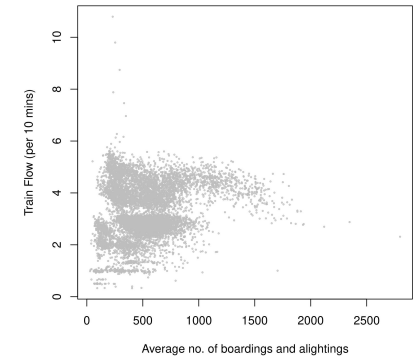
(d) Shek Kip Mei Station



(e) Prince Edward Station



(f) Mong Kok Station



(g) Yau Ma Tei station

Figure 14: Variation of observed train flow in the upward direction over passenger movements for the stations highlighted in Figure 5.